Available online at www.sciencedirect.com
SCIENCE DIRECT®
Journal of Computational Physics 217 (2006) 248–259
JOURNAL OF COMPUTATIONAL PHYSICS
www.elsevier.com/locate/jcp

Stochastic analysis of transport in tubes with rough walls

Daniel M. Tartakovsky [a,b,*], Dongbin Xiu [c]

[a] *Department of Mechanical and Aerospace Engineering, University of California, San Diego, 9100 Gilman Drive, La Jolla, CA 92093, United States*
[b] *Theoretical Division, Los Alamos National Laboratory, Los Alamos, NM 87545, United States*
[c] *Department of Mathematics, Purdue University, IN 47907, United States*

Received 11 August 2005; received in revised form 11 February 2006; accepted 24 February 2006
Available online 24 April 2006

Abstract

Flow and transport in tubes with rough surfaces play an important role in a variety of applications. Often the topology of such surfaces cannot be accurately described in all of its relevant details due to either insufficient data or measurement errors or both. In such cases, this topological uncertainty can be efficiently handled by treating rough boundaries as random fields, so that an underlying physical phenomenon is described by deterministic or stochastic differential equations in random domains. To deal with this class of problems, we use a computational framework, which is based on stochastic mappings to transform the original *deterministic/stochastic problem in a random domain* into a *stochastic problem in a deterministic domain*. The latter problem has been studied more extensively and existing analytical/numerical techniques can be readily applied. In this paper, we employ both a generalized polynomial chaos and Monte Carlo simulations to solve the transformed stochastic problem. We use our approach to describe transport of a passive scalar in Stokes' flow and to quantify the corresponding predictive uncertainty.

PACS: 02.50.Fz; 47.11.+j; 47.55.Mh

Keywords: Random domain; Stochastic inputs; Differential equations; Uncertainty quantification; Stokes' flow; Dispersion

1. Introduction

Viscous flow in domains bounded by highly irregular or rough surfaces has been a subject of a plethora of analytical and numerical studies. The importance of this subject stems from its universal nature, since surface roughness affects the phenomena as diverse as glacier sliding [1] and micro-electronic-mechanical system (MEMS) technology [2]. Indeed, given a proper spatial resolution, virtually any natural or manufactured surface becomes rough. Most of the existing studies have focused either on the validity of simplified mathematical models, e.g. of the lubrication approximation and Reynolds' equations [3] or the derivation of appropriate

* Corresponding author.
E-mail addresses: dmt@lanl.gov, dmt@ucsd.edu (D.M. Tartakovsky), dxiu@math.purdue.edu (D. Xiu).

0021-9991/$ - see front matter
doi:10.1016/j.jcp.2006.02.029

boundary conditions [4–6] or on the effects of roughness on fluid behavior [7,8]. This study deals with the previously unresolved issue of uncertainty quantification for viscous flow and transport in domains with rough surfaces, whose exact topology cannot be ascertained due to the lack of sufficient information and/or measurement errors.

The emphasis on uncertainty quantification suggests the use of probabilistic descriptions of rough surfaces. Such descriptions allow for more realistic, data-driven representations of surfaces roughness [9]. This is in contrast to deterministic conceptualizations that treat rough boundaries as sinusoidal surfaces [7,8], a surface with a large number of periodically distributed humps [10,6], and self-similar and fractal surfaces [7]. Of course, not every stochastic representation of rough surfaces is conducive to uncertainty quantifications. For example, random fractals [11] or fractional Brownian motion [12], which were used to represent rough surfaces, are not readily amenable to parameterization by data. Likewise, the representation of a rough surface as a Gaussian random field with a linear autocorrelation function [13] might conflict with data. One of the goals of this study is to propose a methodology for uncertainty quantification that is flexible enough to allow for non-trivial probabilistic descriptions of rough surfaces that are determined by data.

The adoption of a probabilistic framework to describe rough surfaces makes even an essentially deterministic problem stochastic. In this paper, we use the computational framework first proposed in [14] that is applicable to a wide class of deterministic and stochastic differential equations defined on domains with random (rough) boundaries. A key component of this framework is the use of robust stochastic mappings to transform an original deterministic or stochastic differential equation defined on a *random domain* into a stochastic differential equation defined on a *deterministic domain*. This allows one to employ well-developed theoretical and numerical techniques for solving stochastic differential equations in deterministic domains. While in [14] we defined the stochastic mappings as numerical solutions of Laplace's equations, here we introduce an analytical mapping. Another important difference is that the present study deals with stochastic parabolic equations, while [14] dealt with deterministic elliptic problems.

In Section 2, we formulate a random domain problem, which describes transport of a passive scalar in Stokes' flow in a tube, whose rough surface is modeled as a random field. Our mathematical model consists of an advection–diffusion equation whose Stokes' velocity is computed via the lubrication approximation [15]. A computational approach that allows us both to predict the dynamics of a passive scalar and to quantify the corresponding predictive uncertainty is presented in Section 3. This approach involves an analytical stochastic mapping, a parameterization of a tube's random surface (Section 3.1), and a numerical solution of the transformed stochastic transport equation by means of the generalized polynomial chaos (Section 3.2). The simulation results and their analysis are reported in Section 4. We conclude by listing in Section 5 a few open issues that remain to be studied.

2. Problem formulation

We consider transport of a passive scalar in a low Reynolds number steady-state flow in a pipe (capillary tube) V with a rough surface ∂V (Fig. 1). The concentration $c(\boldsymbol{x}, t)$ of a passive scalar is described by an advection–diffusion equation,

$$\frac{\partial c}{\partial t} + \nabla \cdot (\mathbf{v}c) = D\nabla^2 c, \qquad x \in V, \quad t > 0, \tag{1}$$

where D is the diffusion coefficient and $\mathbf{v}(\mathbf{x})$ is the velocity of a fluid. In a cylindrical coordinate system (r, ϕ, z), the surface of the pipe can be described by $R = \overline{R} + \gamma(\phi, z)$, where $\overline{R}$ is the radius of the pipe ignoring roughness and $\gamma(\phi, z)$ accounts for the roughness. Assuming the surface of the pipe to be impermeable,

$$\frac{\partial c}{\partial r}(r = R) = 0. \tag{2}$$

The boundary conditions for the concentration at the pipe's inlet ($z = 0$) and outlet ($z = \infty$) are

$$c(r, \phi, 0; t) = C_0, \quad \frac{\partial c(r, \phi, \infty; t)}{\partial z} = 0, \qquad 0 < r < R, \quad 0 \leqslant \phi \leqslant 2\pi, \quad t > 0. \tag{3}$$

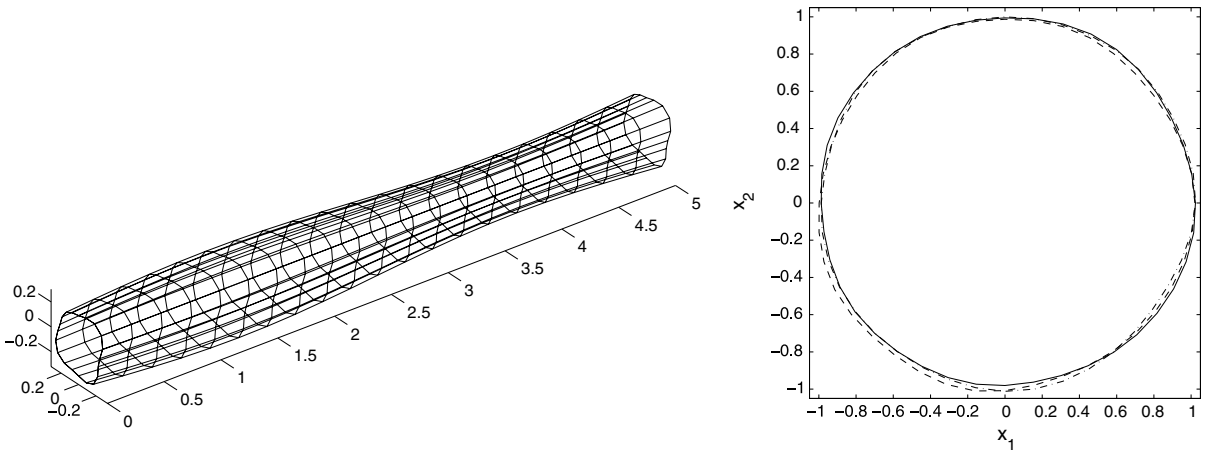

Fig. 1. A schematic representation of a tube whose surface exhibits roughness in both longitudinal (z) and angular (ϕ) directions. The figure on the right shows a few realizations of the tube's cross-section, which is treated as a random field.

The initial concentration is

$$c(r,\phi,z;0)=0, \qquad 0<r<R, \quad 0\leqslant\phi\leqslant 2\pi, \quad z>0. \tag{4}$$

The fluid velocity $\mathbf{v}$ is governed by Stokes' equations,

$$\nabla\cdot\mathbf{v}=0, \quad \text{and} \quad \mu\nabla^2\mathbf{v}=\nabla p, \tag{5}$$

where μ and p denote the viscosity and density of a fluid, respectively. Eqs. (5) are subject to the no-slip boundary condition on the rough walls of the pipe,

$$\mathbf{v}(r=R)=0. \tag{6}$$

Finally, it is assumed that the pressure drop along the pipe is constant,

$$\frac{\mathrm{d}p}{\mathrm{d}z}=-J. \tag{7}$$

Since the surface roughness is much smaller than the radius of the pipe, $\gamma\ll R$, we employ a lubrication approximation [15], which assumes that flow is essentially horizontal ($v_r=v_\phi=0$), so that the direct integration of (5) gives the parabolic distribution of the velocity

$$v_z=J\frac{R^2-r^2}{4\mu}. \tag{8}$$

The accuracy and validity of a similar approximation for flow between two rough plates were investigated numerically in [16,17].

Eqs. (1) and (8) served as a basis for the Taylor's pioneering analysis of solute transport in tubes with smooth walls [18]. In this study, we extend this analysis to account for the wall's roughness. To do so, we treat the surface of the pipe, i.e., $R(\phi,z)$ or, equivalently, $\gamma(\phi,z)$, as a random field. This recasts the advection–diffusion problem (1) and (8) as a stochastic partial differential equation

$$\frac{1}{D}\frac{\partial c}{\partial t}+J\frac{R^2-r^2}{4D\mu}\frac{\partial c}{\partial z}=\frac{1}{r}\frac{\partial}{\partial r}\left(r\frac{\partial c}{\partial r}\right)+\frac{1}{r^2}\frac{\partial^2 c}{\partial\phi^2}+\frac{\partial^2 c}{\partial z^2} \tag{9}$$

defined on the random domain V. In dimensionless form, this problem can be formulated as follows.

Let $\omega\in\Omega$ be a random realization drawn from a complete probability space $(\Omega,\mathscr{A},\mathscr{P})$, whose event space Ω generates its σ-algebra $\mathscr{A}\subset 2^\Omega$ and is characterized by a probability measure $\mathscr{P}$. For all $\omega\in\Omega$, let $V(\omega)\subset\mathbb{R}^3$ be a three-dimensional random domain bounded by boundary $\partial V(\omega)$, some or all of whose

segments are random. For $\mathscr{P}$-almost everywhere (a.e.) in Ω, we look for a stochastic solution $c_d(r_d, \phi, z_d, t; \omega)$ of the advection–diffusion equation

$$\frac{\partial c_d}{\partial t_d} + Pe\frac{R_d^2 - r_d^2}{4}\frac{\partial c_d}{\partial z_d} = \frac{1}{r_d}\frac{\partial}{\partial r_d}\left(r_d\frac{\partial c_d}{\partial r_d}\right) + \frac{1}{r_d^2}\frac{\partial^2 c_d}{\partial \phi^2} + \frac{\partial^2 c_d}{\partial z_d^2} \tag{10}$$

subject to the boundary conditions

$$\frac{\partial c_d}{\partial r_d}(R_d, \phi, z_d, t_d; \omega) = 0, \quad c_d(r_d, \phi, 0, t_d; \omega) = 1, \quad \frac{\partial c_d(r_d, \phi, z_d \gg 1, t_d; \omega)}{\partial z_d} = 0 \tag{11}$$

and the initial condition

$$c_d(r_d, \phi, z_d, 0; \omega) = 0, \qquad 0 < r_d < R_d, \quad 0 \leqslant \phi \leqslant 2\pi, \quad z_d > 0. \tag{12}$$

Here

$$c_d = \frac{c}{C_0}, \quad Pe = \frac{\overline{R}^3 J}{D\mu}, \quad t_d = \frac{Dt}{\overline{R}^2}, \quad r_d = \frac{r}{\overline{R}}, \quad z_d = \frac{z}{\overline{R}}, \quad R_d = 1 + \epsilon, \quad \epsilon = \frac{\gamma}{\overline{R}}. \tag{13}$$

Note that in this formulation, the only source of randomness stems from the wall roughness, i.e., from $R_d(\phi, z_d; \omega) = 1 + \epsilon(\phi, z_d; \omega)$. We assume that $\epsilon(\phi, z_d; \omega)$ is sufficiently regular, and the corresponding boundary conditions are properly posed, to guarantee the well-posedness a.e. $\omega \in \Omega$ of the problem (10)–(12).

3. Computational approach

Following [14], we pursue a computational approach that consists of the following two steps. First, we introduce a one-to-one mapping function that maps the random domain $V(\omega)$ onto a deterministic domain E. Then we solve the resulting stochastic problem in a deterministic domain. Such an approach allows one to use the relatively mature theory of stochastic partial differential equations in fixed deterministic domains to solve differential equations on random domains, the class of problems that has not been systematically analyzed.

In [14], we introduced a stochastic mapping based on solutions of Laplace's equations. Here we explore an analytical mapping

$$r_d = R_d(\xi_2, \xi_3)\xi_1, \qquad \phi = \xi_2, \qquad z_d = \xi_3, \tag{14}$$

which maps random domain $V(\omega)$ onto a deterministic cylinder of unit radius, and the problem (10)–(12) onto a stochastic differential equation (see Appendix A)

$$\frac{\partial c_d}{\partial t_d} + \frac{PeR_d^2}{4}\frac{1 - \xi_1^2}{h_3}\frac{\partial c_d}{\partial \xi_3} = \frac{1}{h_1 h_2 h_3}\left[\frac{\partial}{\partial \xi_1}\left(\frac{h_2 h_3}{h_1}\frac{\partial c_d}{\partial \xi_1}\right) + \frac{\partial}{\partial \xi_2}\left(\frac{h_1 h_3}{h_2}\frac{\partial c_d}{\partial \xi_2}\right) + \frac{\partial}{\partial \xi_3}\left(\frac{h_1 h_2}{h_3}\frac{\partial c_d}{\partial \xi_3}\right)\right] \tag{15}$$

subject to the boundary conditions

$$\frac{\partial c_d}{\partial \xi_1}(1, \xi_2, \xi_3, t_d; \omega) = 0, \quad c_d(\xi_1, \xi_2, 0, t_d; \omega) = 1, \quad \frac{\partial c_d(\xi_1, \xi_2, \xi_3 \gg 1, t_d; \omega)}{\partial \xi_3} = 0 \tag{16}$$

and the initial condition

$$c_d(\xi_1, \xi_2, \xi_3, 0; \omega) = 0. \tag{17}$$

Here ξ_1 is a random variable, ξ_2 and ξ_3 are deterministic, and

$$h_1 = R_d(\xi_2, \xi_3), \quad h_2 = \xi_1\sqrt{\left(\frac{\partial \epsilon}{\partial \xi_2}\right)^2 + R_d^2}, \quad h_3 = \sqrt{\xi_1^2\left(\frac{\partial \epsilon}{\partial \xi_3}\right)^2 + 1}. \tag{18}$$

3.1. Parameterization of random surface

To make computation tractable, we assume that the zero-mean random field $\epsilon(\xi_2, \xi_3; \omega)$ can be approximated by

$$\epsilon(\xi_2, \xi_3; \omega) \approx \epsilon_\phi(\xi_2; \omega)\epsilon_z(\xi_3; \omega), \tag{19}$$

where ϵ_ϕ and ϵ_z are two statistically independent random fields. Then the parameterization of the random surface $R_d = 1 + \epsilon$ consists of the following steps.

First, we represent fluctuation terms as functions of a finite number $K \geqslant 1$ of mutually uncorrelated random variables $Y_1(\omega), \ldots, Y_K(\omega)$ with zero mean and unit variance, so that $\epsilon_\phi(\xi_2; \omega)$ and $\epsilon_z(\xi_3; \omega)$ in (19) can be written as

$$\epsilon_z(\xi_3; \omega) \approx \sum_{k=1}^{K_z} \hat{\epsilon}_{z_k}(\xi_3) Y_k(\omega) \tag{20}$$

and

$$\epsilon_\phi(\xi_2; \omega) \approx \sum_{k=K_z+1}^{K} \hat{\epsilon}_{\phi_k}(\xi_2) Y_k(\omega). \tag{21}$$

The representation (21) and (20) is an approximation, whose accuracy and robustness are the subject of ongoing research in the field of numerical generation of random processes. If these processes are non-Gaussian, this task becomes particularly challenging [19–22]. (In such cases, the goal is often reduced to approximating pointwise marginal distribution functions and two-point covariance functions.) An analysis of the errors induced by the finite-term representations in (21) and (20), as well as of their efficiency, lies beyond the scope of this paper. Instead we refer the interested readers to the references mentioned above.

Second, we choose $\hat{\epsilon}_{z_k}$ and $\hat{\epsilon}_{\phi_k}$ to satisfy prescribed accuracy. One popular choice is the Karhunen–Loève (KL) decomposition [23], which is an optimal decomposition in term of the mean-square approximation error and has been used extensively to represent random inputs [24–26]. Other types of decomposition also can be employed. In this paper, we explore both the KL expansion and a Fourier expansion described below.

3.1.1. Parameterization of the longitudinal roughness

Let the random field $\epsilon_z(\xi_3,\omega)$ have zero mean $\langle \epsilon_z(\xi_3; \omega) \rangle = 0$ and an exponential two-point covariance function

$$C_z(\xi_3, \zeta_3) = \mathbb{E}[\epsilon_z(\xi_3; \omega)\epsilon_z(\zeta_3; \omega)] = \sigma_z^2 \exp\left(-\frac{|\xi_3 - \zeta_3|}{l_z}\right), \tag{22}$$

where σ_z^2 and $l_z > 0$ are the variance and correlation length of the wall roughness in the longitudinal direction, respectively. In the computational examples below, we set $l_z = 1$, which corresponds to a boundary of moderate roughness.

In the finite-term Karhunen–Loève type expansion (20), the expansion coefficients $\{\hat{\epsilon}_{z_k}\}_{k=1}^{K_z}$ are given by $\hat{\epsilon}_{z_k}(\xi_3) = \sqrt{\lambda_{z_k}}\psi_{z_k}(\xi_3)$, where $\{\lambda_{z_k}, \psi_{z_k}(\xi_3)\}$ are the eigenvalues and eigenfunctions of the integral equations

$$\int C_z(\xi_3, \zeta_3)\psi_{z_k}(\zeta_3)\mathrm{d}\zeta_3 = \lambda_{z_k}\psi_{z_k}(\xi_3), \quad k = 1, \ldots, K_z. \tag{23}$$

Then the decomposition (20) becomes

$$\epsilon_z(\xi_3; \omega) \approx \sigma_z \sum_{k=1}^{K_z} \hat{\epsilon}_{z_k}(\xi_3) Y_k(\omega) = \sigma_z \sum_{k=1}^{K_z} \sqrt{\lambda_{z_k}}\psi_{z_k}(\xi_3) Y_k(\omega). \tag{24}$$

We set $\{Y_k(\omega)\}_{k=1}^{K_z}$ to be independent random variables uniformly distributed on $(-1, 1)$, and use the parameter $0 < \sigma_z < 1$ to control the maximum deviation of the rough surface.

It is worthwhile to stress again that the expansion (24) introduces two sources of errors – errors due to the finite K_z-term truncation and errors due to the assumption of independence of $\{Y_k(\omega)\}$. The latter errors

vanish for Gaussian processes, for which the lack of correlation is equivalent to independence. In our simulations, extensive tests were conducted to conclude that $K_z = 4$ is sufficient to obtain results that are independent of resolution (in terms of the number of the KL modes).

3.1.2. Parameterization of the angular roughness

Let the random field $\epsilon_\phi(\xi_2;\omega)$ have zero mean $\langle\epsilon_\phi(\xi_2;\omega)\rangle = 0$ and its statistics be *rotationally invariant* on the circle, i.e., $\langle\epsilon_\phi(\xi_2;\omega)\epsilon_\phi(\zeta_2;\omega)\rangle = C_\phi(|\xi_2 - \zeta_2|)$. Since the random field $\epsilon(\xi_2;\omega)$ is periodic, a natural form of (21) is given by a Fourier type expansion

$$\epsilon_\phi(\xi_2;\omega) \approx \sigma_\phi \sum_{n=-N}^{N} \epsilon_{\phi_n}(\omega)\mathrm{e}^{-\mathrm{i}n\xi_2}, \tag{25}$$

where $0 < \sigma_\phi < 1$ specifies the maximum angular roughness, and the coefficients $\epsilon_{\phi_n}(\omega) = \epsilon^{\mathrm{r}}_{\phi_n}(\omega) + \mathrm{i}\epsilon^{\mathrm{i}}_{\phi_n}(\omega)$ are complex random variables. It is straightforward to show that if the real $(\epsilon^{\mathrm{r}}_{\phi_n})$ and imaginary $(\epsilon^{\mathrm{i}}_{\phi_n})$ components are both statistically independent for all n and have variances $C_n/4$, where

$$C_n = \frac{1}{\pi}\int_0^{2\pi} C_\phi \cos(n\theta)\,\mathrm{d}\theta \tag{26}$$

are the coefficients of the Fourier cosine series of the covariance function C_ϕ, then the random field $\epsilon_\phi(\xi_2,\omega)$ in (25) approximates the prescribed covariance function C_ϕ.

A 2π-periodic covariance function $C_\phi(|\xi_2 - \zeta_2|)$ is constructed by extending the standard Gaussian covariance function $C_{\mathrm{G}} = \exp[-(\xi_2 - \zeta_2)^2/l_\phi^2]$ to the periodic domain $(0, 2\pi)$, where l_ϕ is the correlation length of angular roughness. Fig. 2(a) shows such a periodic covariance function and contrasts it with the standard non-periodic Gaussian covariance function. Fig. 2(b) demonstrates the decay of the Fourier cosine coefficients $\{C_n\}$ for the periodic covariance function with the correlation length $l_\phi = 0.5$. Based on the decay of C_n, we choose $N = 8$ ($C_9 = 0.0052$, $C_1 = 0.2821$, $C_9/C_1 < 2\%$).

In the following examples, we take the coefficients $\epsilon^{\mathrm{r}}_{\phi_n}(\omega)$ and $\epsilon^{\mathrm{i}}_{\phi_n}(\omega)$ in the expansion (25) to be independent random variables uniformly distributed on $(-1, 1)$ for all $n = 0, \ldots, N$. This results in a 17-dimensional ($K - K_z = 2N + 1 = 17$) random space. Combined with the $K_z = 4$ random dimensions from the KL model of the longitudinal roughness, this results in a 21-dimensional ($K = 21$) random space. Below we use $\mathbf{Y} = (Y_1, \ldots, Y_K)^{\mathrm{T}}$ to denote the 21-dimensional random vector.

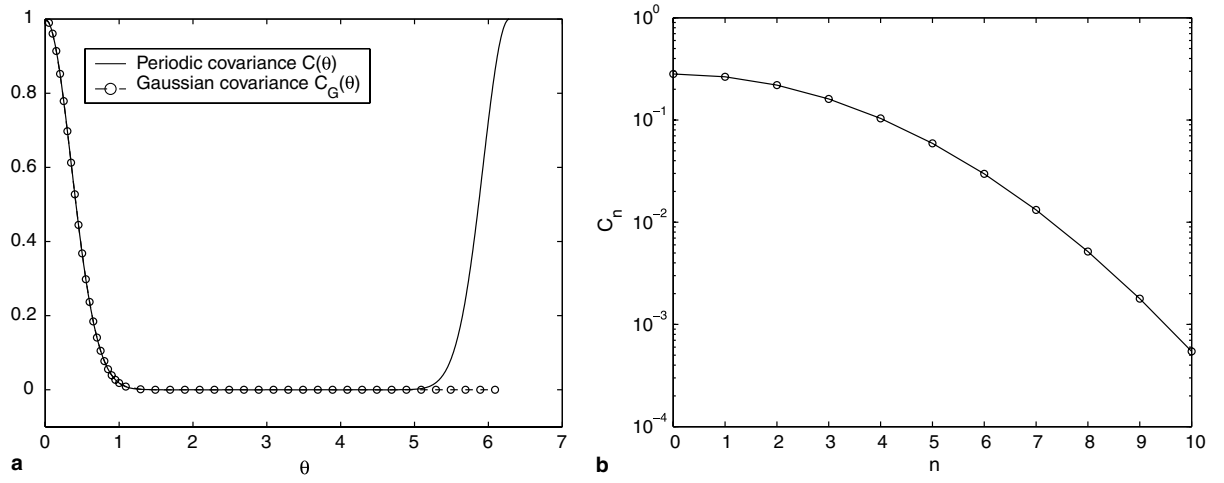

Fig. 2. (a) Periodic covariance function $C_\phi(\xi_2)$ (solid line) based on the non-periodic Gaussian function $C_{\mathrm{G}} = \exp(-\xi^2/l_\phi^2)$ with $l_\phi = 0.5$ (dashed line with circles). (b) Decay of the Fourier cosine coefficients of the periodic covariance function.

3.2. Numerical solutions of the transformed equations

Since the stochastic mapping (14) is represented by (24) and (25) as a function of $\mathbf{Y}$, the metrics terms and the Jacobian corresponding to the coordinate transformation from $x_d = (r_d, \phi, z_d)$ to $\xi = (\xi_1, \xi_2, \xi_3)$ become functions of $\mathbf{Y}$ as well. For example, the Jacobian takes the form

$$J(\xi;\omega) \equiv \frac{\partial(r_d, \phi, z_d)}{\partial(\xi_1, \xi_2, \xi_3)} = R_d(\xi, \mathbf{Y}). \tag{27}$$

Hence, according to the Doob–Dynkin lemma [27], a solution of the problem (15)–(18) can be described by the same set of random variables, i.e.,

$$c_d(x_d, t_d; \omega) = c_d(x_d, t_d; \mathbf{Y}). \tag{28}$$

To facilitate numerical implementation, we follow the standard practice (e.g. [24,26,28] and references therein) and assume that random variables $\{Y_k(\omega)\}_{k=1}^K$ are mutually independent.

The generalized polynomial chaos (gPC) represents c_d in (28) as

$$c_d(x_d, t_d; \omega) = \sum_{j=1}^{M} a_j(x_d, t_d)\Phi_j[\mathbf{Y}(\omega)], \tag{29}$$

where $\{\Phi_j\}$ are (multi-dimensional) orthogonal polynomials of the random vector $\mathbf{Y}(\omega)$, which satisfy the orthogonality relation

$$\langle \Phi_i \Phi_j \rangle = \langle \Phi_i^2 \rangle \delta_{ij}. \tag{30}$$

Here δ_{ij} is the Kronecker delta, and the ensemble average of $\Phi_i\Phi_j$ is defined by the inner product

$$\langle \Phi_i(\mathbf{Y})\Phi_j(\mathbf{Y}) \rangle = \int \Phi_i(\mathbf{Y})\Phi_j(\mathbf{Y})w(\mathbf{Y})\mathrm{d}\mathbf{Y}, \tag{31}$$

with $w(\mathbf{Y})$ denoting a weighting function. If P is the order of the polynomials $\{\Phi_j\}$ that satisfies accuracy requirements, then M, the number of terms in the expansion (29), is defined by $M = (K+P)!/K!P!$. There exists a one-to-one correspondence between the type of the orthogonal polynomials $\{\Phi_i\}$ and the type of the random variable $\mathbf{Y}$. A few types of the gPC corresponding to the commonly used distributions are listed in Table 1 (see [29] for a detailed discussion).

Traditional implementations of the gPC relies on a Galerkin procedure and results in stochastic Galerkin algorithms. In these algorithms, (29) is substituted into (10)–(12), and the resulting equations are projected onto each gPC basis to ensure that the truncation errors are orthogonal to the subspace of $\{\Phi_i\}$. While the gPC-Galerkin approach was successfully applied to various stochastic problems, e.g. [24–26], it often results in a (large) system of coupled equations for each gPC expansion coefficients. This is particularly the case in solving (15), where the presence of the metrics terms complicates the direct Galerkin projection.

As an alternative, we adopt a gPC-collocation method, which typically consists of repetitive runs of a deterministic solver on a set of prescribed (deterministic) nodal points, and results in a completely uncoupled system of equations. Hence, its implementation is trivial and parallelization straightforward. The choice of nodal points is critical. While in one random dimension the choices are abundant (e.g. quadrature points of orthogonal polynomials), the problem becomes much more challenging in multiple dimensions. Indeed,

Table 1
Correspondence between the type of the gPC and the underlying random variables

Random variable $\mathbf{Y}$	gPC basis $\{\Phi(\mathbf{Y})\}$	Support
Gaussian	Hermite	$(-\infty, \infty)$
γ	Laguerre	$[0, \infty)$
β	Jacobi	$[a, b], b > a \in \mathbb{R}$
Uniform	Legendre	$[a, b], b > a \in \mathbb{R}$

construction of the tensor product becomes unfeasible, since the total number of nodes in a K-dimensional space is m^K (where m is the number nodes used in one dimension) grows fast for $K \gg 1$.

We use the approach proposed in [30], where the Smolyak sparse grid is used as nodal points. It has been shown in [30] that such a method is highly efficient for (nonlinear) stochastic differential equations. The gPC-collocational approach retains many properties of the high-order polynomial approximation of gPC-Galerkin, and the total number of nodes grows weakly with respect to the number of random dimensions. For large dimensions $K \gg 1$, the number of nodes scales as $2^P M = 2^P(K+P)!/K!P!$, where P is the polynomial order. The factor 2^P is independent of the dimension K, and therefore the nodal set can be regarded as "optimal". A detailed description of the stochastic collocation method, including its error estimate and numerical properties, can be found in [30].

4. Simulation results

The quantity most readily measured and analyzed in the laboratory setting is the concentration averaged over a cross-section in the tube $A(z_d;\omega)$,

$$c_{av}(z_d,t_d;\omega)=\frac{1}{A}\int_0^{2\pi}\int_0^{R_d} c_d r_d\,dr_d\,d\phi,\quad A(z_d;\omega)=\frac{1}{2}\int_0^{2\pi} R_d^2\,d\phi. \tag{32}$$

In the transformed coordinate system (32) is given by

$$c_{av}(\xi_3,t_d;\omega)=\frac{1}{A}\int_0^{2\pi} R_d\int_0^{1} c_d\xi_1\,d\xi_1\,d\xi_2,\quad A(\xi_3;\omega)=\frac{1}{2}\int_0^{2\pi} R_d^2\,d\xi_2. \tag{33}$$

In all simulations, we set the Peclet number $Pe = 50$. Spatial discretizations are the Fourier collocation in the angular direction and the fourth-order central difference in the remaining two directions. The second-order Crank–Nicolson scheme is used as a temporal scheme. Spatial and temporal steps are chosen based on extensive numerical tests that guarantee that solutions are resolution independent. In the analysis below, we focus on the transitional regime, i.e., on the early time ($t_d \leqslant 2.5$) behavior of the concentration c_d in the region close to the inlet ($0 \leqslant z_d \leqslant 2$).

Fig. 3 shows the first two ensemble moments of the concentration $c_{av}(z_d,t_d)$, i.e., its mean and standard deviation (STD). The mean concentration profile remains practically unchanged for the degree of roughness varying between 0% and 5% of the tube's radius. This leads to a conclusion that, for this degree of roughness, the roughness-induced dispersion of a passive scalar can neglected if one is interested in the mean behavior alone. However, as we demonstrate below, roughness is important for uncertainty quantification.

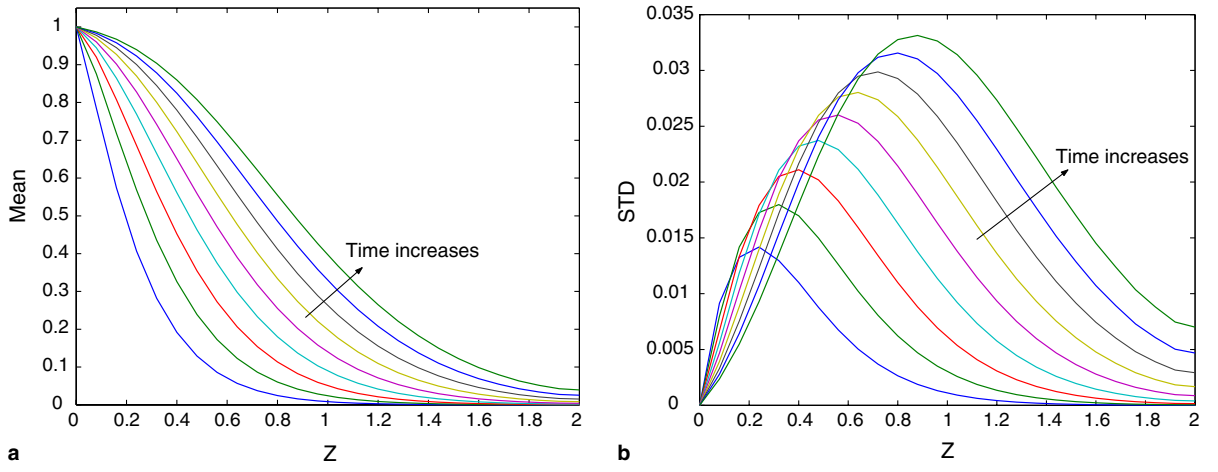

Fig. 3. The mean (a) and standard deviation (b) of the concentration, computed with the generalized polynomial chaos expansion. The roughness parameters are $\sigma_\phi = 2\%$ and $\sigma_z = 5\%$.

The STD shown in Fig. 3(b) allows one to estimate the uncertainty associated with the prediction of concentration dynamics in Fig. 3(a). Deterministic boundary and initial conditions (11) and (12) imply the precise knowledge of both the concentration profile c_d at time t_d and its value at the inlet $z_d = 0$ for all $t_d \geqslant 0$. As one would expect, the predictive uncertainty increases with time and the distance from the inlet. These results are visualized in Fig. 4.

To ascertain the errors introduced by our numerical procedure, we compare in Fig. 5 the standard deviation (STD) computed by means of the generalized polynomial chaos (gPC) with that computed by means of Monte Carlo simulations (MCS). The two approaches give qualitatively similar uncertainty estimates (as expressed by STD). The difference between the two solutions decreases with the number of Monte Carlo realizations.

As observed earlier, the mild roughness (<5%) of a tube's surface does not affect the mean behavior of a passive scalar. However, it has a pronounced effect on uncertainty quantification. Fig. 6, on which three families of the STD curves corresponding to different σ_ϕ and σ_z are shown, demonstrates this effect. As should be expected, the increase in the surface roughness (i.e., in σ_ϕ and σ_z) leads to the increase in predictive

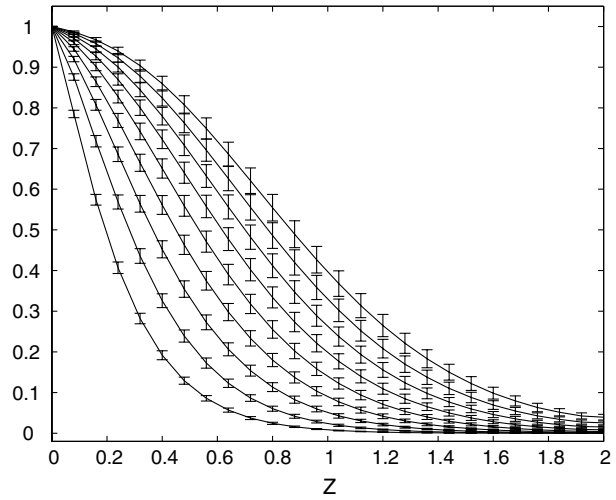

Fig. 4. Prediction of the time evolution of concentration with the corresponding error bars. The roughness parameters are $\sigma_\phi = 2\%$ and $\sigma_z = 5\%$.

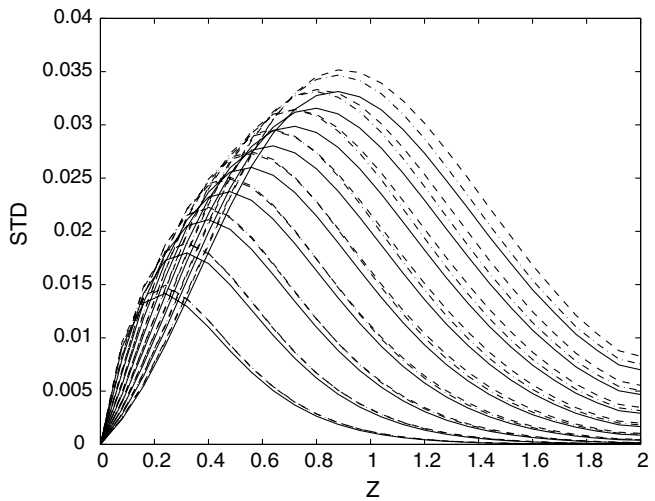

Fig. 5. The STD profiles computed with the generalized polynomial chaos (solid lines) and with 100 (dashed lines) and 500 (dash-dotted lines) realizations of Monte Carlo simulations. The roughness parameters are $\sigma_\phi = 2\%$ and $\sigma_z = 5\%$.

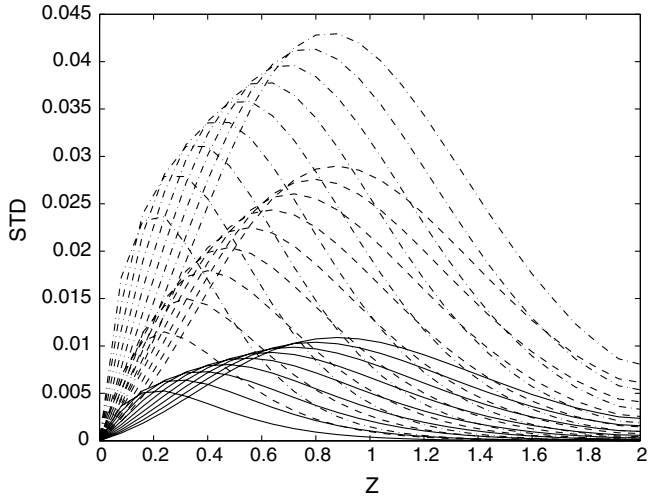

Fig. 6. Families of the STD profiles corresponding to several degrees of roughness: $\sigma_\phi = 1\%$ and $\sigma_z = 1\%$ (solid lines), $\sigma_\phi = 1\%$ and $\sigma_z = 5\%$ (dashed lines), and $\sigma_\phi = 5\%$, $\sigma_z = 1\%$ (dash-dotted lines).

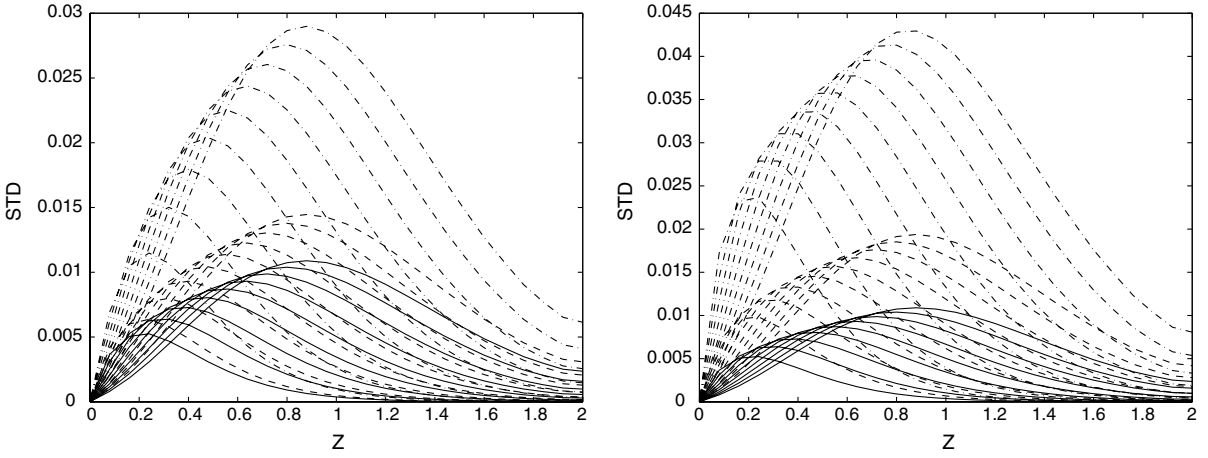

Fig. 7. Relative effect of uncertainty in angular and longitudinal roughness. The first set of the STD profiles corresponds to a fixed $\sigma_\phi = 1\%$ and several values σ_z, i.e., $\sigma_z = 1\%$ (solid lines), to $\sigma_z = 2\%$ (dashed lines) and $\sigma_z = 5\%$ (dash-dotted lines). The second set of the STD profiles corresponds to a fixed $\sigma_z = 1\%$ and several values σ_ϕ, i.e., $\sigma_\phi = 1\%$ (solid lines), to $\sigma_\phi = 2\%$ (dashed lines) and $\sigma_\phi = 5\%$ (dash-dotted lines).

uncertainty. The uncertain angular roughness (σ_ϕ) contributes more to predictive uncertainty than the uncertain longitudinal roughness does. The latter point is elucidated further in Fig. 7.

5. Summary

We used the computational framework of Xiu and Tartakovsky [14] to predict transport of a conservative scalar in a tube, whose rough surface is under-specified by data and is modeled as a random field. A key component of this approach is the use of stochastic mappings to transform the original problem into a (better understood) problem of stochastic equations in deterministic domains. While our previous analysis [14] relied on a mapping defined by numerical solutions of the Laplace equations, here we propose and implement an analytical mapping. Another key difference is that here we use the mean domain (a cylinder in the case of a tube) as a mapping target, rather than a canonical domain (such as a square) used in [14].

This random mapping enables us to apply the existing numerical methods for the resulting transformed stochastic equations in fixed domains. Here we used the generalized polynomial chaos expansions, although we emphasize that other suitable techniques can be used. The analytical nature of the proposed stochastic mapping enabled us to consider a transient three-dimensional advection–diffusion equation. We found that

- The effects of low to moderate roughness (the normalized standard deviation of the surface roughness below 5%) on mean dispersion of a passive scalar are negligible.
- The predictive uncertainty increases with time. Its maximum propagates away from the inlet, where concentration is fixed and deterministic.
- The effects of the angular roughness (roughness in the ϕ direction) are more prominent than those of the axial roughness (roughness in the z direction).

It remains to investigate the effects of more severe degrees of roughness. The challenges involved are both computational and conceptual:

- A more realistic description of the roughness, which replaces (19) with a fully two-dimensional random field representation of a tube's surface $R(z,\phi;\omega)$.
- The surface roughness, whose standard deviation significantly exceeds 5% and exhibits short correlation lengths, increases the number of terms in the generalized polynomial chaos expansion, thus increasing the computational burden.
- Under conditions of severe roughness, the validity of the lubrication approximation (8) might break down. This will necessitate a numerical solution of a system of Stokes' and advection–diffusion equations.

Acknowledgments

The work of the first author was performed at Los Alamos National Laboratory (LA-UR-04-5497) under the auspices of the National Nuclear Security Agency of US Department of Energy under contract W-7405-ENG-36. It was supported in part by the US Department of Energy under the DOE/BES Program in the Applied Mathematical Sciences, Contract KC-07-01-01, and in part by the LDRD Program at Los Alamos National Laboratory.

Appendix A. Stochastic domain mapping

Consider a transformation of coordinates $(r,\phi,z)\to(\tilde r,\tilde\phi,\tilde z)$ such that $r=f_r(\tilde r,\tilde\phi,\tilde z)\equiv R(\tilde\phi,\tilde z)\tilde r$, $\phi=f_\phi(\tilde r,\tilde\phi,\tilde z)\equiv\tilde\phi$ and $z=f_z(\tilde r,\tilde\phi,\tilde z)\equiv\tilde z$. The corresponding diagonal metric tensor is $g_{ij}=g_{ii}\delta_{ij}$, where δ_{ij} is the Kronecker delta. Since $x=\tilde rR(\tilde\phi,\tilde z)\cos\tilde\phi$, $y=\tilde rR(\tilde\phi,\tilde z)\sin\tilde\phi$ and $z=\tilde z$, the scale factors are given by

$$h_r\equiv h_{ii}=\sqrt{g_{ii}}=\sqrt{\left(\frac{\partial x}{\partial\tilde r}\right)^2+\left(\frac{\partial y}{\partial\tilde r}\right)^2+\left(\frac{\partial z}{\partial\tilde r}\right)^2}=R(\tilde\phi,\tilde z),\tag{A.1}$$

$$h_\phi\equiv h_{22}=\sqrt{g_{22}}=\sqrt{\left(\frac{\partial x}{\partial\tilde\phi}\right)^2+\left(\frac{\partial y}{\partial\tilde\phi}\right)^2+\left(\frac{\partial z}{\partial\tilde\phi}\right)^2}=\tilde r\sqrt{\left(\frac{\partial\epsilon}{\partial\tilde\phi}\right)^2+R^2},\tag{A.2}$$

and

$$h_z\equiv h_{22}=\sqrt{g_{22}}=\sqrt{\left(\frac{\partial x}{\partial\tilde z}\right)^2+\left(\frac{\partial y}{\partial\tilde z}\right)^2+\left(\frac{\partial z}{\partial\tilde z}\right)^2}=\sqrt{\tilde r^2\left(\frac{\partial\epsilon}{\partial\tilde z}\right)^2+1}.\tag{A.3}$$

In the new coordinate system $(\tilde r,\tilde\phi,\tilde z)$, the gradient and Laplacian operators are given by

$$\nabla=\tilde{\mathbf r}\frac{1}{h_r}\frac{\partial}{\partial\tilde r}+\tilde{\boldsymbol\phi}\frac{1}{h_\phi}\frac{\partial}{\partial\tilde\phi}+\tilde{\mathbf z}\frac{1}{h_z}\frac{\partial}{\partial\tilde z}\tag{A.4}$$

and

$$\triangle = \frac{1}{h_r h_\phi h_z}\left[\frac{\partial}{\partial \tilde{r}}\left(\frac{h_\phi h_z}{h_r}\frac{\partial}{\partial \tilde{r}}\right) + \frac{\partial}{\partial \tilde{\phi}}\left(\frac{h_r h_z}{h_\phi}\frac{\partial}{\partial \tilde{\phi}}\right) + \frac{\partial}{\partial \tilde{z}}\left(\frac{h_r h_\phi}{h_z}\frac{\partial}{\partial \tilde{z}}\right)\right], \tag{A.5}$$

respectively.

References

[1] J.F. Nye, A calculation on the sliding of ice over a wavy surface using a Newtonian viscous approximation, Proc. R. Soc. Lond. A 311 (1969) 445–467.
[2] W.A. Gross, Fluid Film Lubrication, Wiley, London, 1980.
[3] S.R. Brown, H.W. Stockman, S.J. Reeves, Applicability of the Reynolds equation for modeling fluid flow between rough surfaces, Geophys. Res. Lett. 22 (18) (1995) 2537–2540.
[4] M.J. Miksis, S.H. Davis, Slip over rough and coated surfaces, J. Fluid Mech. 273 (1994) 125–139.
[5] K. Sarkar, A. Prosperetti, Effective boundary conditions for Stokes flow over a rough surface, J. Fluid. Mech. 316 (1996) 223–240.
[6] W. Jäger, A. Mikelić, On the roughness-induced effective boundary conditions for an incompressible viscous flow, J. Diff. Equations 170 (2001) 96–122.
[7] C. Pozrikidis, Unsteady viscous flow over irregular boundaries, J. Fluid Mech. 255 (1993) 11–34.
[8] D.L. Jacono, F. Plouraboue, A. Bergeon, Weak-inertial flow between two rough surfaces, Phys. Fluids 17 (2005) 063602-1–063602-10.
[9] J. Rudzitis, V. Padamans, E. Bordo, R. Haytham, Random process model of rough surfaces contact, Meas. Sci. Technol. 9 (7) (1998) 1093–1097.
[10] K.M. Jansons, Determination of the macroscopic (partial) slip boundary condition for a viscous flow over a randomly rough surface with a perfect slip microscopic boundary condition, Phys. Fluids 31 (1) (1988) 15–17.
[11] M.G. Blyth, C. Pozrikidis, Heat conduction across irregular and fractal-like surfaces, Int. J. Heat Mass Transf. 46 (8) (2003) 1329–1339.
[12] M. Madadi, M. Sahimi, Lattice boltzmann simulation of fluid flow in fracture networks with rough, self-affine surfaces, Phys. Rev. E (Statistical, Nonlinear, and Soft Matter Physics) 67 (2) (2003) 26309-1.
[13] S.R. Harp, R.F. Salant, An average flow model of rough surface lubrication with inter-asperity cavitation, J. Tribol. 123 (2001) 134–143.
[14] D. Xiu, D.M. Tartakovsky, Numerical methods for differential equations in random domains, SIAM J. Sci. Comput. 27 (3) (2005) 1118–1139.
[15] G.K. Batchelor, An Introduction to Fluid Dynamics, Cambridge Univ. Press, Cambridge, 1967.
[16] S.R. Brown, Fluid flow through rock joints: The effect of surface roughness, J. Geophys. Res 92 (1987) 1337–1347.
[17] V.V. Mourzenko, J.F. Thovert, P.M. Adler, Permeability of a single fracture: Validity of the Reynolds equation, J. Phys. II France 5 (1995) 465–482.
[18] G.I. Taylor, Dispersion of soluble matter in solvent flowing slowly through a tube, Proc. Roy. Soc. London, Ser. A 219 (1137) (1953) 186–2003.
[19] M. Grigoriu, Simulation of stationary non-Gaussian translation processes, J. Eng. Mech. 124 (2) (1998) 121–126.
[20] S. Sakamoto, R. Ghanem, Simulation of multi-dimensional non-gaussian non-stationary random fields, Prob. Eng. Mech. 17 (2002) 167–176.
[21] M. Shinozuka, G. Deodatis, Simulation of stochastic processes by spectral representations, Appl. Mech. Rev. 44 (1991) 191–203.
[22] F. Yamazaki, M. Shinozuka, Digital generation of non-Gaussian stochastic fields, J. Eng. Mech. 114 (7) (1988) 1183–1197.
[23] M. Loève, Probability Theory, fourth ed., Springer, 1977.
[24] I. Babuška, R. Tempone, G. Zouraris, Galerkin finite element approximations of stochastic elliptic differential equations, SIAM J. Numer. Anal. 42 (2004) 800–825.
[25] R. Ghanem, P. Spanos, Stochastic Finite Elements: A Spectral Approach, Springer, 1991.
[26] D. Xiu, G. Karniadakis, Modeling uncertainty in steady state diffusion problems via generalized polynomial chaos, Comput. Methods Appl. Math. Engrg. 191 (2002) 4927–4948.
[27] B. Oksendal, Stochastic Differential Equations. An Introduction With Applications, fifth ed., Springer, Berlin, 1998.
[28] O. Le Maitre, H. Najm, R. Ghanem, O. Knio, Multi-resolution analysis of Wiener-type uncertainty propagation schemes, J. Comput. Phys. 197 (2004) 502–531.
[29] D. Xiu, G. Karniadakis, The Wiener-Askey polynomial chaos for stochastic differential equations, SIAM J. Sci. Comput. 24 (2) (2002) 619–644.
[30] D. Xiu, J.S. Hesthaven, High order collocation methods for differential equations with random inputs, SIAM J. Sci. Comput. (2006), in press.